

Numerical Study of a Pipe Extension Effect in Draft Tube on Hydraulic Turbine Performance

Jafar Nejadali^a *, Alireza Riasi^b

^a Department of Mechanical Engineering, Faculty of Engineering and Technology, University of Mazandaran, Babolsar, Iran

^b School of Mechanical Engineering, University of Tehran, Tehran, Iran

ARTICLE INFO

Article history:

Received: 2 October 2019

Accepted: 1 May 2020

Keywords:

CFD simulation

Hydraulic turbine

Draft tube

Cavitation

Pressure recovery factor

ABSTRACT

Draft tube of Francis type hydraulic turbine usually consists of: cone, elbow and diffuser. On the contrary, in some power stations an extra pipe should be added to the draft tube at the bottom of cone because of installation limitation. In this paper, this special case has been numerically studied. To this end CFD analysis was applied to simulate all parts of hydraulic turbine. A homogeneous multiphase model with Rayleigh-Plesset cavitation model was applied for presence of cavitation. The results reveal that the additional tube causes pressure drop and severe cavitation at the trailing edge of runner blades. Also, results showed that the efficiency reduces in comparison with original hill-diagram of model test in which this extension was not considered. With the removal of the extension tube, the efficiency increased significantly. The comparison of pressure recovery factors along draft tube, and theoretical investigation showed that the height of the draft tube is an important parameter and addition of an extra pipe will cause reduction in draft tube performance and increases the probability of occurrence of cavitation under the runner.

1. Introduction

The use of hydropower for electricity production began in the late eighteenth century. Small hydroelectric power plants are accepted as a beneficial factor in renewable energy. In developed countries, small hydropower plants are just a supplementary in the production of clean renewable energy. But in developing countries, can play an important role in supply of electricity. Hydraulic turbine is the main part of hydro power stations. Therefore, its optimal operation will have a desirable effect on performance of hydropower plants. Mismatch between the performance of hydroelectric power plants and the presented hill-chart is one of the wide spread problems for some hydroelectric power plants. One of the main reasons for these differences is the change occurs in turbine configuration during installation. Although, these changes apparently are small but their effect will be considerable.

Numerical simulation of fluid flow is one of the best methods for evaluating hydroelectric power plants performance. During recent decades, with the expansion of computer power, computational fluid dynamics (CFD), as one of the stages of design process, reduced time and costs [1, 2].

Many tasks associated with the simulation of flow in hydraulic turbine were performed in recent years for performance prediction, cavitation detection and also transient flow simulation. Mohammadi et al. studied the effect of water, air and

their combined injection from two different injection points to reduce vorticity effects in a draft tube of prototype turbine working using CFD [3]. Yang et al. carried out a numerical simulation to Explore the swirling flow variations in the non-cavitation flow and cavitation flow field to explain the mechanism of the complex unsteady flow in the draft tube. They found that there are mutual influences between the swirling flow and cavitation [4, 5]. Tania et al. carried out CFD analyzes to obtain a draft tube geometry that improves the hydrodynamic performance of the GAMM Francis turbine. They found that the draft tube in hyperbolic-logarithmic spiral format has the highest efficiency and the draft tube in logarithmic spiral format has the lowest loss coefficient [6]. Shojaeefard et al. discussed the shape optimization of draft tubes utilized in Agnew type micro-hydro turbines, with the aim of maximizing the pressure recovery factor and minimizing the energy loss coefficient of flow [7]. Foroutan et al. developed a new RANS turbulence model in order to predict the mean flow field in a draft tube operating under partial load using a 2-D axisymmetric model [8]. Nam et al. combined the computation fluid dynamic (CFD) and the design of experiment (DOE) to improve performance of the hydraulic turbine draft tube in its design process [9]. Demirel et al. presented a design optimization study of an elbow type draft tube based on the combined use of Computational Fluid Dynamics (CFD), design of experiments, surrogate models and multi-objective optimization. It is determined that, pressure recovery factor can be increased by 4.3%, and head loss can be reduced by %20 compared to the initial

* Corresponding author. Tel.: +9-811-313-1437; e-mail: j.nejad@umz.ac.ir

CFD aided design [10]. The swirling flow at the outlet of a Francis turbine runner has a major influence on the overall behavior of the flow downstream in the draft tube. Based on this idea, Resiga et al. carried out an experimental and theoretical investigation in order to elucidate the causes of a sudden drop in the draft tube pressure recovery coefficient at a discharge near the best efficiency operating [11].

A draft tube of a Francis type hydraulic turbine usually consists of: cone, elbow and diffuser. In some power stations, because of installation limitation an extension (which is a cylindrical tube in this case) should be added to the draft tube. In this case, the surplus pipe located at the bottom of cone. It is well mentioning that the model test of the power station has been performed without of this extension and the extra pipe added later during prototype installation because of some space restriction. The main objectives of this paper are: (a) study the effect of this extension on turbine performance using full CFD analysis of the hydraulic turbine, (b) multiphase flow analysis of turbine to consider cavitation conditions.

Table 1. Specifications of the turbine

Conditions	Value
Runner diameter	2760 mm
Number of runner blades	17
Number of stay vanes	24
Number of guide vanes	26
Runner rotational speed	250 rpm
Draft tube style	Elbow draft tube

2. Turbine components

Three-dimensional geometries of all components of Francis turbine including spiral casing, stay vanes, guide vanes and draft tube are generated using relevant technical documentations. Parameters of the prototype turbine is shown in Table 1. The general assembly of this turbine is shown in Fig. 1 and the cone extension is specified.

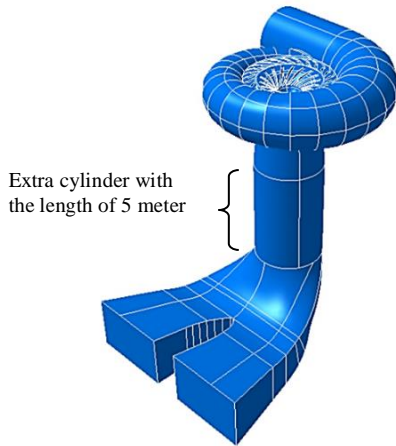


Figure 1. 3D geometry of all components of Francis turbine.

3. Numerical scheme and model description

A 3D CFD code was applied as the solver. Reynolds-averaged Navier-Stokes (RANS) equations are solved using Ansys-CFX. The governing equations used are the continuity equation (eq. (1)) and the momentum equation (eq. (2)).

$$\frac{\partial \rho_m}{\partial t} + \frac{\partial(\rho_m u_j)}{\partial x_j} = 0 \quad (1)$$

$$\frac{\partial(\rho_m u_i)}{\partial t} + \frac{\partial(\rho_m u_j u_i)}{\partial x_j} = -\frac{\partial P}{\partial x_i} + \quad (2)$$

$$\frac{\partial}{\partial x_j} \left[(\mu_m + \mu_t) \left(\frac{\partial u_i}{\partial x_j} + \frac{\partial u_j}{\partial x_i} \right) \right] - \rho_m \omega u_i - \rho_m \omega (\omega r)$$

The mixture density ρ_m and the mixture dynamic viscosity μ are defined as;

$$\rho_m = \rho_v \alpha_v + \rho_l (1 - \alpha_v) \quad (3)$$

$$\mu = \mu_v \alpha_v + \mu_l (1 - \alpha_v) \quad (4)$$

The liquid-vapor mass transfer due to cavitation governed by the vapor volume fraction transport is expressed by the eq. (5) [12].

$$\frac{\partial(\rho_v \alpha)}{\partial t} + \frac{\partial(\rho_v \alpha u_j)}{\partial x_j} = \dot{m}_v + \dot{m}_c \quad (5)$$

For turbulence modeling, RNG $k - \epsilon$ model has been applied which is more responsive to streamline curvature and higher strain rates than the standard one [8, 10, 13]. The governing equations are discretized using the finite element finite volume method in the code. The high resolution scheme was applied for discretization of momentum equation, pressure, turbulent kinetic energy, and turbulent dissipation rate [14].

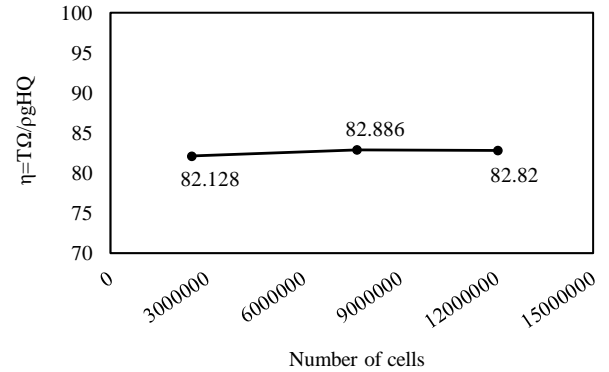


Figure 2. Efficiency versus number of cells

For grid generation of the models described above, tetrahedral mesh is used near the walls and hexahedral mesh is generated in regions with small pressure gradient. A size function has been employed in order to lower the mesh number. Size function starts from a small mesh size and increases with a growth rate. This function is a desirable strategy to obtain refined mesh in regions where large pressure gradients are expected such as boundary layer. During mesh generation, orthogonal quality, skewness, and aspect ratio are assured to be in desirable range. As shown in Fig. 2, for grid independency studies, three adapted grid sizes, were assessed. Grid independency was established at around 7.6×10^6 cells. The generated meshes are shown in Fig. 3.

All walls are defined as non-porous and with standard roughness, the fluid selected was standard water liquid at 20 °C and the gravity is included in the operating conditions. The reference pressure was assumed to be zero and the vapor pressure of the water was set to 2338 Pa. The fluid flow was assumed steady state. Mass flow rate at spiral casing inlet and average static pressure at draft tube outlet were assumed for the boundary conditions. The information is tabulated in Table 2.

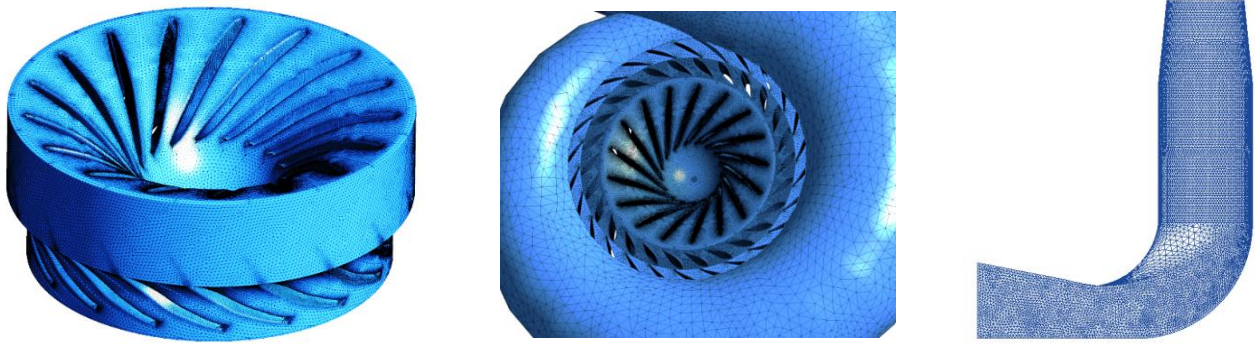


Figure 3. Computational grid for parts of turbine.

Table 2. Information of CFD simulation

Features	Descriptions
Walls	No slip, with standard roughness
Reference pressure	0 Pa
Vapor pressure	2338 Pa
Analysis Type	Steady state, Two phase
Fluid type	Water (liquid and vapor)
Inlet boundary condition	Mass flow rate (inlet of spiral casing)
Outlet boundary condition	Average static pressure (outlet of draft tube)

The present research considers five operating points for each opening of guide vanes. The simulations were performed from spiral casing to the end of draft tube. The pressure at the outlet of draft tube was calculated with eq. (6) for all operating points [3].

$$\frac{P_{avg,out}}{\gamma} = \frac{P_a}{\gamma} + Z \quad (6)$$

In this equation, Z is the distance between the center line of the draft tube outlet and the tail-race. The spiral case, stay vanes, guide vanes and draft tube domains were stationary and the runner domain was rotating at constant speed. The grids between impeller and spiral case are connected by means of a frozen rotor interface. Conservation of mass was checked on the interfaces between the runner computational domain and computational domains corresponding to the fixed parts. For numerical simulation, the convergence criteria were set at maximum residuals of 10^{-4} .

4. Results and discussion

The dimensionless parameters in hydraulic Turbines are defined as follows:

$$\phi = \frac{Q}{ND^3} \quad (7)$$

$$\psi = \frac{gH}{(ND)^2} \quad (8)$$

$$\hat{P} = \frac{P}{\rho N^3 D^5} \quad (9)$$

The efficiency of Francis turbine is defined as:

$$\eta = \frac{P}{P_r} \quad (10)$$

The results of CFD analysis of the main hydraulic turbine (with an extension under the cone of draft tube) at full opening of wicket

gate (wicket gate opening is measured relative to full closing state and the maximum angle is about 27°) were compared with the data of model testing (without any extension under the cone of draft tube) in Fig. 4. As it can be seen, the power coefficient was in good agreement with experimental data (the maximum error was about 0.7%), while efficiency at the BEP is about 10% lower than Model test results. It should be mentioned that the geometry of the runner was extracted from spare part and there is the possibility of a slight difference between the main and spare runner.

Variations of efficiency and power coefficient versus flow coefficient for different opening of guide vanes are shown in Fig. 5. As it can be seen the best efficiency occurs at 60% opening of guide vanes.

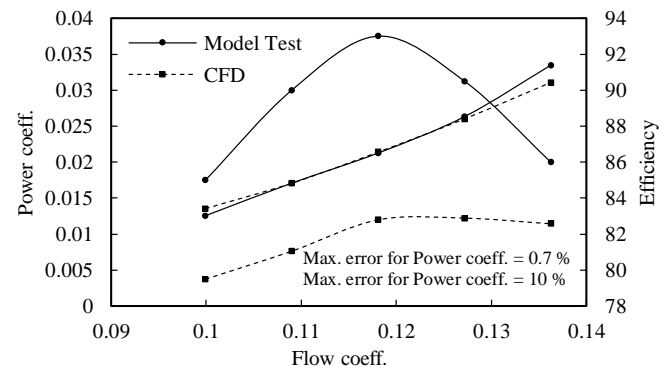


Figure 4. Variation of Power coefficient and efficiency versus volume flow rate at 100% opening of GV

4.1. Presence of cavitation

Cavitation is a fundamental phenomenon that occurs in flowing liquids. It may occur when the local static pressure in a fluid goes below the vaporization pressure of the liquid at the actual temperature. In the case of hydraulic-turbines it is, usually, an

undesirable phenomenon because in most cases it implies negative effects such as losses, efficiency reduction, noise, erosion and vibration [15]. As this purpose, two-phase simulation was performed for this case. A homogeneous multiphase model with Rayleigh-Plesset cavitation model was applied for presence of cavitation. The results showed that cavitation may occur in an extensive area of runner particularly at the trailing edge. This is clearly shown in Fig. 6 by using gas volume fraction contours. Regarding different types of cavitation in Francis turbines, that is of the type of traveling bubble at the trailing edge cavitation [16, 17]. It seems that the pressure reduction is very pronounced at the runner outlet and it is reinforced by using an extra cylindrical tube with the length of 5 meters under the cone of draft tube that is indicated in Fig. 1. To have deep insight of this effect, the extension was removed from draft tube and simulation was repeated. The results for the both cases have been compared to each other in Fig. 7. As can be seen in Fig. 6 and Fig. 7 use of this extra cylindrical tube causes reduction of pressure under the runner which results intense cavitation at the trailing edge. It occurs in most of turbine operating conditions and eventually leads to loss of efficiency. Results of numerical simulation for the case without extension pipe showed that the efficiency at the operating point was increased about 7 % relative to the case with extension pipe.

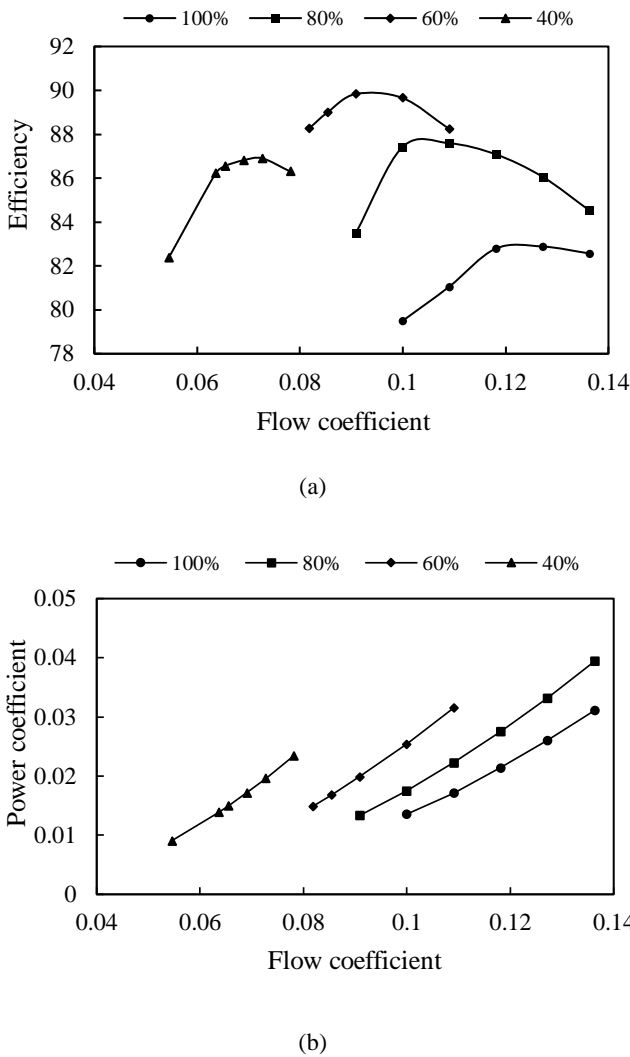


Figure 5. a) Efficiency versus flow coefficient. b) Power coefficient versus flow coefficient, at different opening of GV

In Fig. 6 and Fig. 7, there is a region under the cone of runner where the vapor is formed. This phenomenon is often termed as vortex breakdown leading to the formation of a helical vortex rope in the draft tube [18, 19]. The creation of a vortex rope in the flow through a draft tube leads to pressure fluctuations on the wall. These oscillations create vibrations and, if the frequency of these oscillations coincides with the natural frequency of the structure, this leads to resonance [3]. Axial and circumferential velocity distribution in one meter below the centerline of the turbine at two opening of guide vanes (100% and 60%), for both cases (with and without extension pipe) are shown in Fig. 8 and Fig. 9.

The results showed that there were not any significant changes in the vortex area in two cases. However, there is a reduction in the strength of the vortex for the case of without extension pipe, at 60% opening of guide vanes.

4.2. Pressure recovery

A significant quantity of kinetic energy leaves the runner in reaction turbines. The amount of kinetic energy that is converted to pressure energy at the runner exit defines the performance of the draft tube [20, 21]. In this study, the pressure recovery factor, C_p (eq. (11)) was applied in order to evaluate the performance of draft tube. It is a common engineering parameter used to measure the amount of kinetic energy recovered along the draft tube.

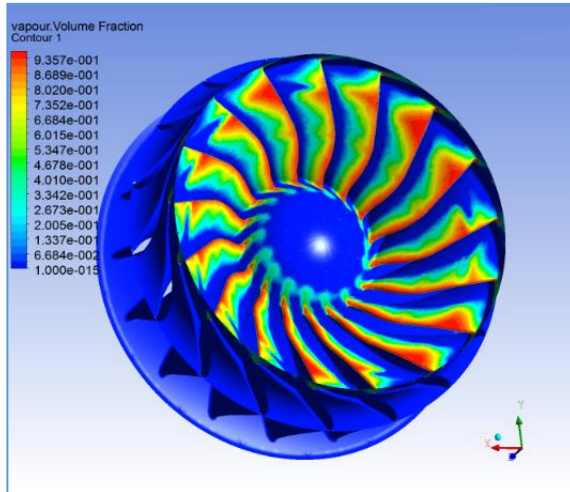
$$C_p = \frac{2 (P_s - P_{s-in})}{\rho (Q/A_{in})^2} \quad (11)$$

Measurement locations of draft tube are indicated in Fig. 10. Figure 11 represents the comparison of pressure recovery factors along the draft tube with extension tube and without extension tube. As can be seen, in both cases the pressure recovery factor increases up to the end of the cone region. In the region of extension pipe, there is not any significant change in C_p and it remains constant and starts to increase in the elbow region. It is obvious from Fig. 11 that by removing the cylindrical tube, the pressure recovery factor is increasing continuously along the draft tube. The results showed that the pipe extension will have negative effect on the performance of the draft tube and eventually will reduce the efficiency of the turbine. The reduction in efficiency was shown in Fig. 4. The wall pressure recovery (eq. (12)) is an estimation of draft tube efficiency. In practice, the hydraulic performance of a turbine draft tube is quantified with the wall pressure recovery coefficient [21].

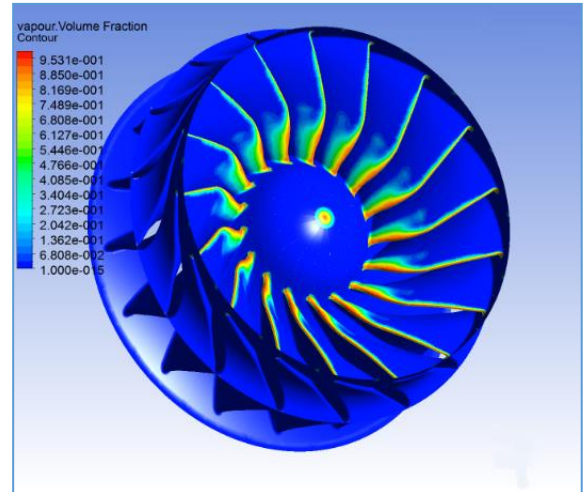
$$C_{P-wall} = \frac{2 (P_w - P_{w-in})}{\rho (Q/A_{in})^2} \quad (12)$$

The wall pressure recovery (C_{P-wall}) variations along the upper and lower paths in the draft tube is illustrated in Fig. 12a and Fig. 12b for two cases. As can be seen in these figures, C_{P-wall} along the upper side is increasing in the cone and reduces in the elbow region as expected because of the acceleration of flow towards the inner radius of the elbow. Conversely, the wall pressure recovery factor along the lower side starts to increase along the elbow region because of the increase in static pressure due to the deceleration of flow towards the outer radius of the elbow. In Fig. 12a, there is a significant reduction in C_{P-wall} along the upper side, because of the existence of extension tube which is lead to inadequate function of the draft tube.

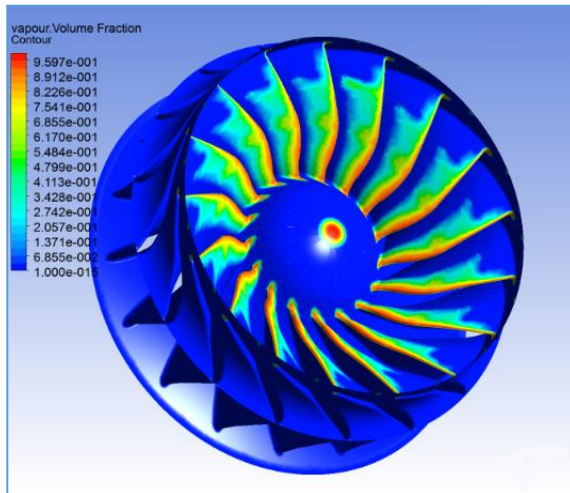
The wall pressure recovery (C_{P-wall}) variations along the upper and lower paths in the draft tube is illustrated in Figures 11 and 12 for two cases.



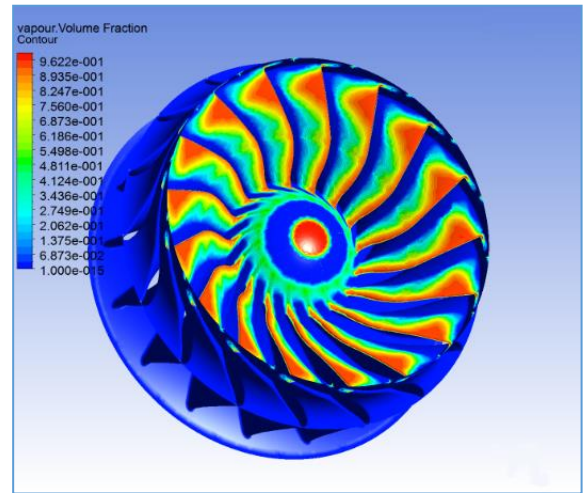
$$\phi/\phi_n = 0.78$$



$$\phi/\phi_n = 0.93$$

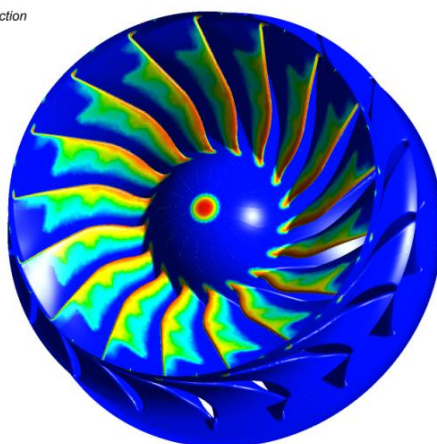
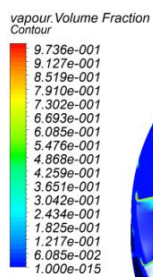


$$\phi/\phi_n = 1$$

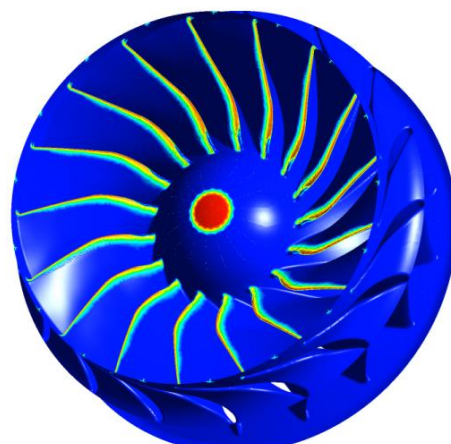


$$\phi/\phi_n = 1.15$$

Figure 6. Contours of volume fraction in runner (guide vane opening of 100%)



(a)



(b)

Figure 7. Contours of volume fraction in runner at nominal condition (a) With extension tube (b) Without extension tube

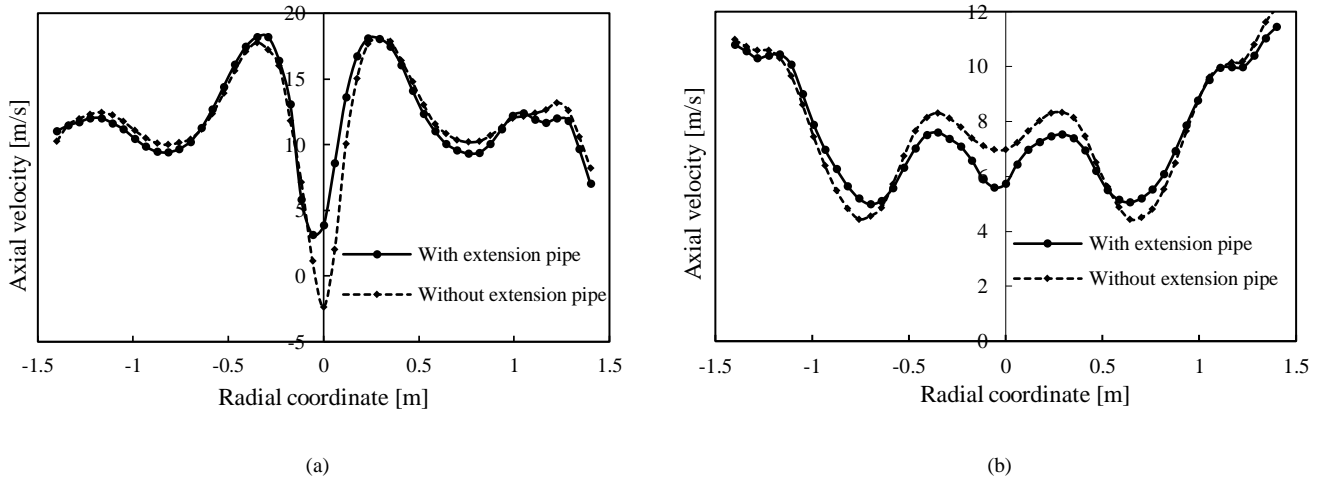


Figure 8. Axial velocity distribution in one meter below the centerline: a) 100% opening of guide vanes. b) 60% opening of guide vanes

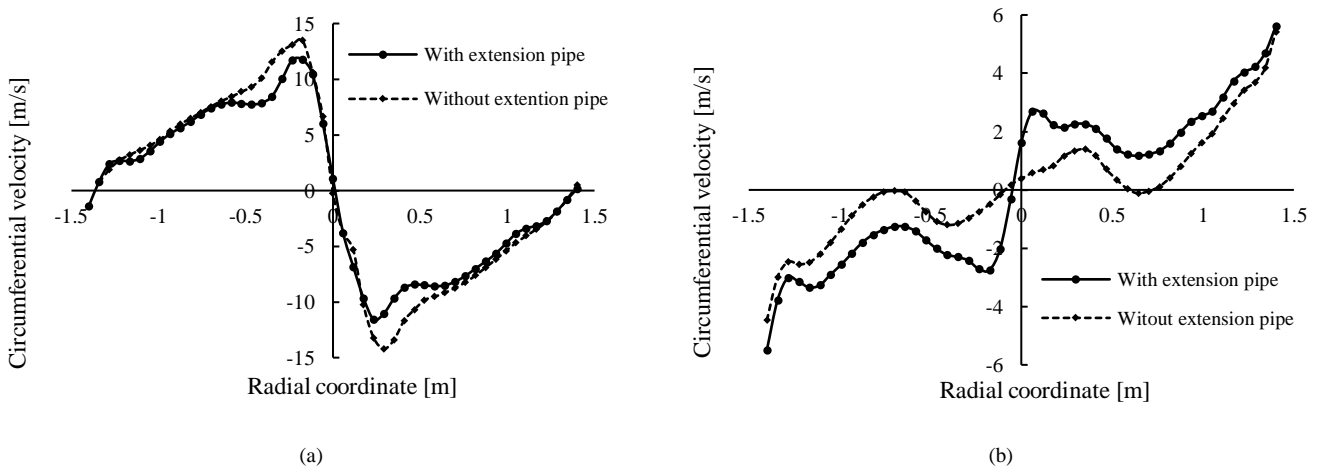


Figure 9. Circumferential velocity distribution in one meter below the centerline: a) 100% opening of guide vanes. b) 60% opening of guide vanes

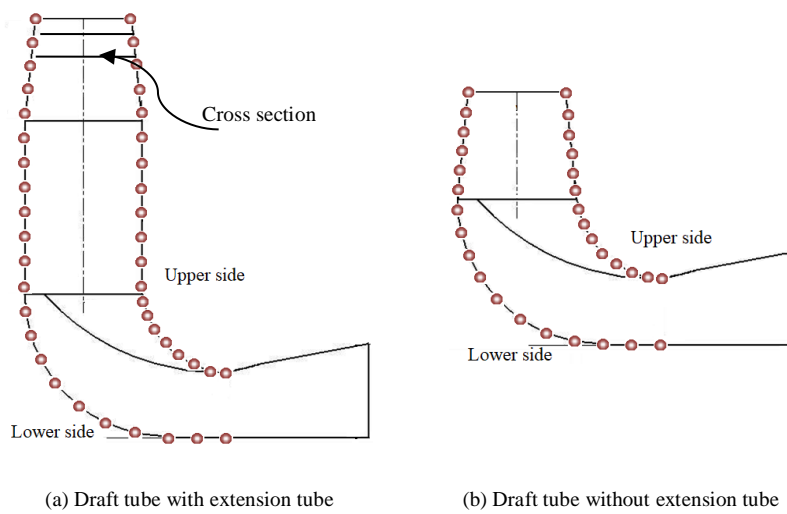


Figure 10. Measurement locations of draft tubes

As can be seen in these Figures, $C_{p, wall}$ along the upper side is increasing in the cone and reduces in the elbow region as expected

because of the acceleration of flow towards the inner radius of the elbow.

Conversely, the wall pressure recovery factor along the lower side starts to increase along the elbow region because of the increase in static pressure due to the deceleration of flow towards the outer radius of the elbow. In Figure 11, there is a significant reduction in C_{P-wall} along the upper side, because of the existence of extension tube, which is lead to inadequate function of the draft tube.

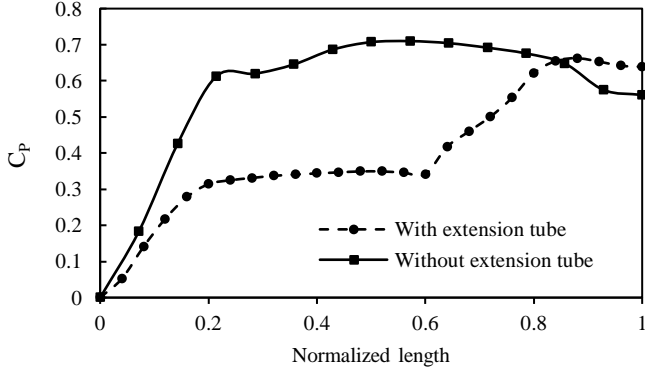
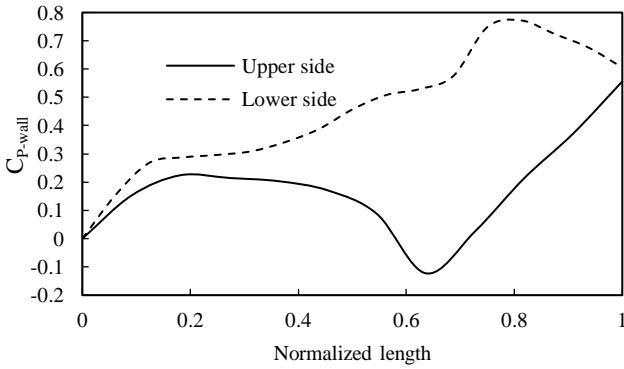
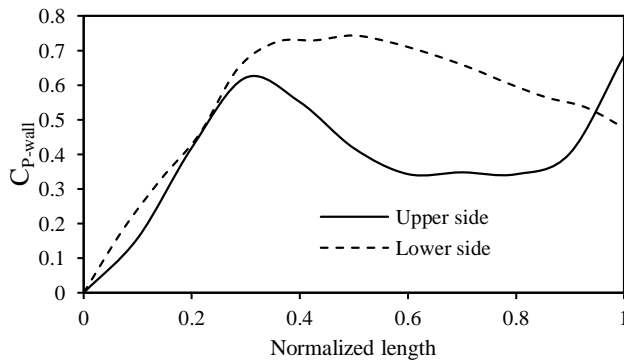


Figure 11. The comparison of Pressure recovery factor obtained from CFD calculations



(a)



(b)

Figure 12. Wall Pressure recovery factor for draft tube a) with extension tube, b) without extension tube

4.3. Theoretical point of view

Writing the energy equation between point A (below runner) and point B (outlet of draft tube) for the draft tube with extension tube based on the Figure 13, we have:

$$\frac{P_A}{\rho g} + Z_A + \frac{\alpha_A V_A^2}{2g} = \frac{P_B}{\rho g} + Z_B + \frac{\alpha_B V_B^2}{2g} + h_{draft} \quad (13)$$

Since draft tube is a diffuser, V_B is always less than V_A which implies the second term of the above relation is always negative. P_B is the gauge pressure. Thus the above relation can be reduced to the following:

$$\left(\frac{P_{A-absolute}}{\rho g} \right)_{With\ extension} = - \left[Z_A + \frac{\alpha_A V_A^2 - \alpha_B V_B^2}{2g} - h_{draft} \right] \quad (14)$$

According to the eq. (14), the amount of absolute pressure in region A will always be negative. Doing the same procedure for the draft tube without extension tube, we will have:

$$\left(\frac{P_{A-absolute}}{\rho g} \right)_{Without\ extension} = - \left[(Z_A - Z_{B'}) + \frac{\alpha_A V_A^2 - \alpha_B V_{B'}^2}{2g} - h'_{draft} \right] \quad (15)$$

It is obvious that $Z_{B'}$ is equal to the length of extension pipe. h'_{draft} can be estimated using the classic relationship of loss in the pipes.

$$h'_{draft} = h_{draft} - 2fL \frac{Q^2}{\pi d^3 g} \quad (16)$$

Substitution of eq. (16) into eq. (15):

$$\left(\frac{P_{A-absolute}}{\rho g} \right)_{With\ extension} = \left(\frac{P_{A-absolute}}{\rho g} \right)_{Without\ extension} - L + 2fL \frac{Q^2}{\pi d^3 g} \quad (17)$$

For the fluid to flow into the tube, the amount of hydraulic loss in the pipe should not be greater than the length (L) of the pipe. Equation (17) shows that the pipe extension leads to a reduction in absolute pressure in region A and consequently, the probability of occurrence of cavitation under the runner increases. Thus height of the draft tube is an important parameter to avoid cavitation.

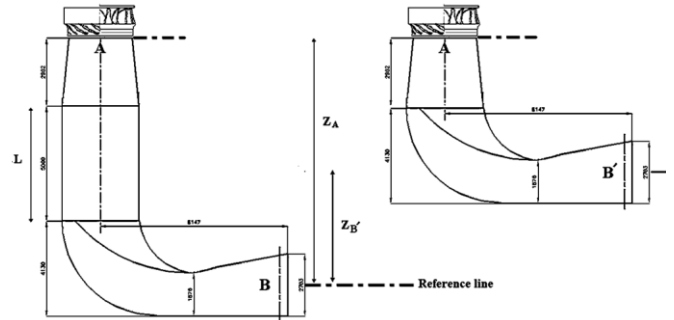


Figure 13. Schematics of draft tubes. With extension (left) and without extension (right)

5. Conclusion

Because of installation limitation, in some power stations an extra pipe should be added to the draft tube at the bottom of the cone. In this paper, Computational Fluid Dynamic (CFD) was applied to study and evaluate the effect of this extra pipe on the performance of Francis hydraulic turbine in power stations. In order to investigate the presence of cavitation, a homogeneous multiphase model with Rayleigh-Plesset cavitation model was applied. Contours of Gas Volume Fraction (GVF), showed that use of this extra cylindrical tube caused reduction of pressure under the runner which resulted intensive cavitation at the trailing edge of the runner blades. It was occurred in most of turbine operating conditions. It was found from the comparison of pressure recovery factor, that the pipe extension will have negative effect on the

performance of the draft tube and eventually will reduce the efficiency of the turbine. It was not observed any significant changes in the vortex area for two cases. Eventually, the issue was studied from a theoretical point of view. The result reveal that the pipe extension leads to a reduction in absolute pressure under the runner and consequently, the probability of occurrence of cavitation in this region increases.

Acknowledgments

The authors acknowledge the support of Hydraulic Machinery Research Institute of University of Tehran.

References

[1] H. Keck, M. Sick, Thirty years of numerical flow simulation in hydraulic turbomachines, *Acta mechanica*, Vol. 201, No. 1-4, pp. 211-229, 2008.

[2] J. Hellström, B. Marjavaara, T. Lundström, Parallel CFD simulations of an original and redesigned hydraulic turbine draft tube, *Advances in Engineering Software*, Vol. 38, No. 5, pp. 338-344, 2007.

[3] M. Mohammadi, E. Hajidavalloo, M. Behbahani-Nejad, Investigation on Combined Air and Water Injection in Francis Turbine Draft Tube to Reduce Vortex Rope Effects, *Journal of Fluids Engineering*, Vol. 141, No. 5, pp. 051301, 2019.

[4] J. Yang, Q. Hu, Z. Wang, J. Ding, X. Jiang, Effects of inlet cavitation on swirling flow in draft-tube cone, *Engineering Computations*, Vol. 35, No. 4, pp. 1694-1705, 2018.

[5] J. Yang, L. Zhou, Z. Wang, The numerical simulation of draft tube cavitation in Francis turbine at off-design conditions, *Engineering Computations*, Vol. 33, No. 1, pp. 139-155, 2016.

[6] T. M. Arispe, W. de Oliveira, R. G. Ramirez, Francis turbine draft tube parameterization and analysis of performance characteristics using CFD techniques, *Renewable energy*, Vol. 127, pp. 114-124, 2018.

[7] M. H. Shojaeefard, A. Mirzaei, A. Babaei, Shape optimization of draft tubes for Agnew microhydro turbines, *Energy conversion and management*, Vol. 79, pp. 681-689, 2014.

[8] H. Foroutan, S. Yavuzkurt, An axisymmetric model for draft tube flow at partial load, *Journal of Hydrodynamics*, Vol. 28, No. 2, pp. 195-205, 2016.

[9] M. chol Nam, B. Dechun, Y. Xiangji, J. Mingri, Design optimization of hydraulic turbine draft tube based on CFD and DOE method, in *Proceeding of*, IOP Publishing, pp. 012019.

[10] G. Demirel, E. Acar, K. Celebioglu, S. Aradag, CFD-driven surrogate-based multi-objective shape optimization of an elbow type draft tube, *International Journal of Hydrogen Energy*, Vol. 42, No. 28, pp. 17601-17610, 2017.

[11] R. Susan-Resiga, G. D. Ciocan, I. Anton, F. Avellan, Analysis of the swirling flow downstream a Francis turbine runner, *Journal of Fluids Engineering*, Vol. 128, No. 1, pp. 177-189, 2006.

[12] P. Gohil, R. Saini, Numerical Study of Cavitation in Francis Turbine of a Small Hydro Power Plant, *Journal of Applied Fluid Mechanics*, Vol. 9, No. 1, 2016.

[13] K. Anup, Y. H. Lee, B. Thapa, CFD study on prediction of vortex shedding in draft tube of Francis turbine and vortex control techniques, *Renewable energy*, Vol. 86, pp. 1406-1421, 2016.

[14] J. Nejad, A. Riasi, A. Nourbakhsh, Parametric study and performance improvement of regenerative flow pump considering the modification in blade and casing geometry,

International Journal of Numerical Methods for Heat & Fluid Flow, Vol. 27, No. 8, pp. 1887-1906, 2017.

[15] M. Morgut, D. Jošt, A. Škerlavaj, E. Nobile, G. Contento, Numerical Predictions of Cavitating Flow Around a Marine Propeller and Kaplan Turbine Runner with Calibrated Cavitation Models, *Strojniski Vestnik/Journal of Mechanical Engineering*, Vol. 64, No. 9, 2018.

[16] F. Avellan, *Introduction to cavitation in hydraulic machinery*, Politehnica University of Timișoara, pp. 2004.

[17] H. Zhang, L. Zhang, Numerical simulation of cavitating turbulent flow in a high head Francis turbine at part load operation with OpenFOAM, *Procedia Engineering*, Vol. 31, pp. 156-165, 2012.

[18] R. Goyal, M. J. Cervantes, B. K. Gandhi, Vortex rope formation in a high head model Francis turbine, *Journal of Fluids Engineering*, Vol. 139, No. 4, pp. 041102, 2017.

[19] R. Susan-Resiga, S. Muntean, A. Stuparu, A. Bosioc, C. Tănasă, C. Ighişan, A variational model for swirling flow states with stagnant region, *European Journal of Mechanics-B/Fluids*, Vol. 55, pp. 104-115, 2016.

[20] B. Mulu, M. Cervantes, C. Devals, T. Vu, F. Guibault, Simulation-based investigation of unsteady flow in near-hub region of a Kaplan Turbine with experimental comparison, *Engineering Applications of Computational Fluid Mechanics*, Vol. 9, No. 1, pp. 139-156, 2015.

[21] R. Susan-Resiga, S. Muntean, V. Hasmatuchi, I. Anton, F. Avellan, Analysis and prevention of vortex breakdown in the simplified discharge cone of a Francis turbine, *Journal of Fluids Engineering*, Vol. 132, No. 5, pp. 051102, 2010.

Nomenclature

A_m	Cross section at inlet of draft tube (m^2)
C_P	Pressure recovery factor
D	Runner outer diameter (m)
d	Extension pipe diameter (m)
f_i	External force (kgm^{-2})
g	Gravity (ms^{-2})
H	Total head of turbine (m)
h	Hydraulic loss (m)
L	Length of Extension pipe (m)
m_c	Condensation mass transfer rate (kgs^{-1})
m_v	Evaporation mass transfer rate (kgs^{-1})
N	Rotational speed (min^{-1})
P	Power (kgm^2s^{-2})
P_a	Ambient pressure (Pa)
P_{avg}	Average static pressure (Pa)
P_w	Wall static pressure (Pa)
P_T	Total input Power (kgm^2s^{-2})
P	Power coefficient
Q	Volume flow rate (m^3s^{-1})
T	Torque on shaft (kgm^2s^{-2})
u_i	$[u, v, w]$, Instantaneous velocity vector
x_i	$[X, Y, Z]$, Cartesian coordinates
Z	Height (m)
α_v	Vapor volume fraction
η	Efficiency
ρ	Density (kgm^{-3})
ρ_l	Liquid density (kgm^{-3})
ρ_v	Vapor density (kgm^{-3})
ρ_m	Mixture density (kgm^{-3})

ν	<i>Kinematic viscosity ($m^2 s^{-1}$)</i>
μ	<i>Dynamic viscosity ($kgm^{-1}s^{-1}$)</i>
μ_l	<i>Liquid dynamic viscosity ($kgm^{-1}s^{-1}$)</i>
μ_T	<i>Turbulent viscosity ($kgm^{-1}s^{-1}$)</i>
μ_v	<i>Vapor dynamic viscosity ($kgm^{-1}s^{-1}$)</i>
ϕ	<i>Flow coefficient</i>
ϕ_n	<i>Nominal Flow coefficient</i>
ψ	<i>Head coefficient</i>
Ω	<i>Rotational speed ($rad s^{-1}$)</i>
ω	<i>Turbulent frequency</i>